NASA Technical Memorandum 82833

Compression Behavior of Unidirectional Fibrous Composites

J. H. Sinclair and C. C. Chamis
Lewis Research Center
Cleveland, Ohio

Prepared for the
Symposium on Compression Testing of Homogeneous Materials and Composites
sponsored by the American Society for Testing and Materials
Williamsburg, Virginia, March 10–11, 1982

NASA

COMPRESSION BEHAVIOR OF UNIDIRECTIONAL FIBROUS COMPOSITES

by J. H. Sinclair* and C. C. Chamis**

National Aeronautics and Space Administration
Lewis Research Center
Cleveland, Ohio 44135

ABSTRACT

The longitudinal compression behavior of unidirectional fiber composites is investigated using the Illinois Institute of Technology Research Institute (IITRI) test method with thick and thin test specimens. The test data obtained is interpreted using the stress/strain curves from back-to-back strain gages, examination of fracture surfaces by scanning electron microscope and predictive equations for distinct failure modes including fiber compression failure, Euler buckling, delamination and flexure. The results show that the longitudinal compression fracture is induced by a combination of delamination, flexure and fiber tier breaks. No distinct fracture surface characteristics can be associated with unique failure modes. An equation is described which can be used to extract the longitudinal compression strength knowing the longitudinal tensile and flexural strengths of the same composite system.

INTRODUCTION

An investigator testing studying the longitudinal compression behavior of unidirectional fiber composites frequently encounters several difficulties. The difficulties are associated with the proper interpretation of the data which in general have considerable scatter. The scatter results primarily from the various failure modes that can induce longitudinal compression failure. The various failure modes that are suspected to induce compression failure include: fiber symmetric and nonsymmetric microbuckling, fiber compression failure, and delamination [1, 2]. The difficulties are compounded because compression testing is sensitive to factors such as Euler buckling, specimen misalignment in the testing fixture, fiber misalignment in the specimen, bending/stretching coupling in the laminate and moisture present in the laminate. Various test methods are used to measure longitudinal compression strength of unidirectional composites. These methods include the Celanese, the Illinois Institute of Technology Research Institute (IITRI) (modified Celanese), the sandwich beam and the face supported beam [3, 4, 5]. Each of these test methods has advantages and disadvantages as well as requiring test specimens unique to the method. The IITRI method is attaining wide use but it is sensitive to several of the factors mentioned previously.

The flexural test (three-point-bend) is used extensively for quality control of composites. This test subjects a test specimen to both longitudinal tension and compression as well as interlaminar shear. The longitudinal tensile strength is determined relatively easily compared to the longitudinal

---

*Materials Engineer.
**Aerospace Structures and Composites Engineer.

compression strength. Also the longitudinal tensile strength can be estimated with reasonable accuracy using the rule of mixtures. It would seem appropriate, then, to investigate the possibility of extracting the longitudinal compression strength of unidirectional composites by using test data from longitudinal tensile strength and from flexural strength for the same composite system. The objective of this investigation is to study the longitudinal compression behavior of unidirectional composites and, thereby, describe an equation which can be used to extract the longitudinal compression strength from tensile and flexural strengths. The IITRI test method is used to test thin and thick specimens. Data obtained from this method are compared with equations which predict longitudinal compression strength based on the specific failure modes mentioned previously. Stress-strain curves from back-to-back strain gages and scanning electron micrographs are examined to identify unique fracture characteristics.

SPECIMEN PREPARATION AND TESTING

Specimen Preparation

Test materials were unidirectional graphite fiber/epoxy resin laminates of AS/PR288 (0.532 fiber volume ratio, and T-300/5208 (0.590 fiber volume ratio). Twelve replicates were cut from each material using a diamond cutting wheel. Dimensions were 4.86 inches (12.34 cm) long by 0.25 inch (0.635 cm) wide. Specimen fiber direction was parallel to the specimen length which was also the compression axis. The ends of the compression specimens were reinforced with adhesively bonded fiber glass tabs. Tab material was 0.041 (0.104 cm thick). Specimen layout plan and a test specimen schematic are shown in figure 1. Each specimen was instrumented with two general purpose 90 degree tee rosette strain gages mounted back-to-back at mid-length center of the 0.50 inch (1.27 cm) long gage section

Testing

A Riehle DS-20 universal test machine was used. It has a screw powered single crosshead weighing system. It is crosshead displacement controlled with speed continuously adjustable from 0.02 to 20 inches per minute. The load cell is a strain gage type with 20,000 lb capacity and a 1 lb resolution.

The compresssion fixture was the fixture originated by IITRI. An instrumented specimen placed in the fixture is shown in figure 2.

Testing order for a given series of specimens was determined by random selection. Crosshead travel velocity for the tests was approximately 0.02 inches per minute. The tests were run incrementally; about 5 seconds were required to record the data at each load increment.

Scanning Electron Microscope Examination

Some of the fractured surfaces were studied by using a scanning electron microscope (SEM). Segments of tested laminates containing the fracture surfaces of interest were cut (while carefully preserving fracture surfaces) from each specimen and cemented (on edge with fracture surface up) to aluminum mounts. In order to facilitate observation by SEM, the specimens were made electrically conductive by coating them with a gold film, approximately

200 Angstroms (20 nm) thick, which was applied by vapor deposition in a vacuum evaporator. They were then studied and photographed with a JUL-JSM-2 scanning electron microscope.

EXPERIMENTAL RESULTS AND DISCUSSION

The experimental results consist of stress-strain data, fracture stresses and strains, combined plots, SEM photographs of some of the fracture surfaces and photographs of selected fractured specimens.

Stress-Strain Data

The strain-gage data reduction program (SGDR) was used to generate stress-strain curves from the incremental loads and corresponding data recorded from strain gages [6].

The measured data for all specimens is summarized in table I. The data shown represents the average value for the two gages and includes modulus along the load direction, Poisson's ratio, fracture stress and fracture strain. Plots of axial stresses (σ_{CXX}) as functions of axial strains (ϵ_{CXX}) for the back-to-back strain gages are shown in figures 3 to 6 for selected specimens of the two materials tested.

The AS/PR288 specimen data shown in table I had a mean compression strength of 128 ksi (882 MPa). The strengths were quite uniform; the standard deviation (s) was 7.6 ksi (52 MPa). Mean fracture strain for these specimens was 0.86 percent with an s of 0.1 percent. Longitudinal modulus (average) was 15.6×10^6 psi (107 GPa) with an s of 1.78×10^6 psi (12 GPa). The mean Poisson's ratio was 0.34; s was 0.02. These tests gave quite uniform results; therefore just one typical stress-strain curve is presented in figure 3. (Again, an SEM study for this specimen is discussed later.) One of the curves suddenly started unloading at about 95 ksi (655 MPa) indicating pronounced bending and possible buckling.

The T-300/5208 specimen data shown in table I had a mean compression strength of 186 ksi (1280 MPa). There was a lot of scatter; strengths ranged between 256 ksi (1760 MPa) and 138 ksi (950 MPa). The standard deviation for the twelve specimens was 47.0 ksi (324 MPa). The mean fracture strain was 1.06 percent with a standard deviation of 0.34. The longitudinal modulus for these specimens ranged between 21.7×10^6 psi (150 GPa) and 17.6×10^6 psi (121 GPa) with a mean value and standard deviation of 19.0×10^6 psi (131 GPa) and 1.23×10^6 psi (8.5 GPa) respectively. The mean value for Poisson's ratio was 0.33 (standard deviation, 0.015). Stress-strain curves for three of the specimens are shown in figures 4, 5, and 6. These represent high, medium and low fracture load specimens respectively. SEM studies (to be discussed later) were also made of fracture surfaces of these three specimens.

Fractured Specimens Characteristics

Some of the T-300/5208 specimens tested are shown in figure 7. They fractured at one end of the test section down into the end tab. Specimens of the other laminate, AS/PR288, also fractured near an end tab but not within the tab itself. These were not photographed.

Scanning Electron Microscope Examination Results

The fractured surfaces of selected specimens were examined using a scanning electron microscope. The ones presented in this report in figures 8 to 11 are from the same specimens for which stress-strain curves are presented. The views of the fracture surfaces of the T-300/5208 specimens are supplemented with a photograph of the broken test specimen taken from figure 7. Figures 8, 9, and 10 are from high-, medium-, and low-load-to-fracture specimens of T-300/5208, respectively. Figure 11 is typical of the fracture surfaces of the AS/PR288 laminate which had small scatter in the compressive strengths of the twelve specimens tested.

In general the surfaces produced by fracturing longitudinal uniaxial graphite/epoxy specimens in the IITRI compression fixture appeared similar to those resulting from tensile fracture of like composites, similarly oriented, in that tiered fractures were produced [7]. But the tiers or stepped surfaces produced by compression fractures appear smoother than those found in tension specimens. Sheared or lacerated resin was observed between fibers on lateral surfaces connecting different tiered or stepped zones. As might be expected fewer fiber pull-outs were found in the compression fractured specimens compared to tensile fractured ones. Resin cleavage was less noticeable in the compression specimens; this may have been partly due to fiber spacing which appeared to be closer than in the areas of the tension specimens examined earlier [7]. Extensive longitudinal cracking of the matrix along the fibers occurred during compression testing. Some of this cracking can be seen in the photographs of the tested T-300/5208 specimens in figure 7. Note the flaring out at the fracture surface. It is not known whether these cracks occurred at the instant of fracture or whether they were caused by further pressure between the fractured segments of the specimen immediately after fracture but before the test machine could be shut off. Such cracks were less commonly found in tensile testing.

In comparing figures 8, 9, and 10, no positive clues associated with the relative strengths of the three specimens which fractured at 253 ksi (1744 Pa), 172 ksi, (1186 MPa) and 145 ksi (1000 MPa) respectively were observed by the authors.

THEORETICAL RESULTS AND COMPARISONS

Governing Equations for Different Failure Modes

Four different methods were used to obtain theoretical predictions of the longitudinal compression strength. This was done in order to assess and to provide a comparison basis for the measured data. The four methods are Euler buckling, flexural strength, delamination, and composites micromechanics via fiber compressive fracture. Each method represents a different longitudinal compression failure mode and provides an independent theoretical estimate of the longitudinal compression strength.

The longitudinal compression strength ($S_{\ell 11C}$) from Euler buckling was predicted using the classical fixed-end column equation

$$S_{\ell 11C} = \frac{4\pi^2 EI}{\ell^2 A} \tag{1}$$

where E is the longitudinal modulus measured in these tests, I is the least moment of inertia ($I = bh^3/12$; b is the specimen width and h the thickness), A is the specimen cross sectional area, and l is the unsupported length at the instant fracture occurred which could be longer than the specimen gage length. The unsupported length will depend on tab debonding at failure.

The longitudinal compression strength from flexural strength was predicted using a three-point-bend simulation and assuming a rectangular stress distribution in the cross-section at fracture. The equation describing this simulation is

$$S_{\ell 11C} = \frac{S_{\ell 11F}}{3 - \frac{S_{\ell 11F}}{S_{\ell 11T}}} \tag{2}$$

where, $S_{\ell 11F}$ is the flexural strength determined from a three-point bend test using the simple beam formula and $S_{\ell 11T}$ is the longitudinal tensile strength. The simulation described by equation (2) was found to provide a reasonable estimate for a variety of composite systems (unpublished Lewis data).

The longitudinal compression strength from delamination controlled by interlaminar (short-beam)shear strength was predicted using the following equation:

$$S_{\ell 11C} = 10\, S_{\ell 12S} + 2.5\, S_{mT} \tag{3}$$

where $S_{\ell 12S}$ is the interlaminar shear strength measured using a short-beam shear test and S_{mT} is the matrix tensile strength. Equation (3) is an empirical curve fit and was found to give reasonable results for a variety of composite systems (unpublished Lewis data).

The longitudinal compression strength from composites micromechanics (controlled by fiber compression strength) was predicted using the equation

$$S_{\ell 11C} = S_{fc}\left(V_f + V_m \frac{E_m}{E_{f11}}\right) \tag{4}$$

where S_{fc} is the fiber compression strength taken to be about 0.9 of the fiber tensile strength, V_f is the fiber volume ratio, V_m is the matrix volume ratio, E_m is the matrix modulus, and E_{f11} is the fiber longitudinal modulus. Compression strength of the graphite fiber is estimated to be about 90 percent of the corresponding tensile strength S_{fT}. Using this estimate and the composite micromechanics equations for longitudinal tensile strength and modulus, equation (4) can be equivalently expressed as

$$S_{\ell 11C} \approx 0.9\, S_{\ell 11T} \tag{5}$$

where $S_{\ell 11T}$ is the longitudinal tensile strength.

In addition to the four methods described above, the longitudinal compression strength was predicted using fiber unsymmetric microbuckling. The

value predicted using this model was about 500 ksi (3450 MPa) which was judged to be unreasonably high compared to literature values of 210 ksi (1447 MPa), [8].

Predictions and Comparisons

The predicted longitudinal compression strengths (using appropriate numerical values from tables 1 and 2, in equations (1), (2), (3), and (5), and a length of 1 in (2.54 cm) in eq. (1)) and the corresponding measured data longitudinal compressive strengths are summarized in figure 12 for the AS/PR288 specimens.

The interesting points to be noted in this figure are: (1) Most of the measured data is close to the strength predicted by the use of flexural and tensile strengths (flexure failure mode eq. (2)). Flexure failure mode appears to provide a lower bound on the measured data. (2) Euler buckling (eq. (1)) and delamination (eq. (2)) predict approximately the same longitudinal compression strength. These two failure modes appear to provide an upper bound on the measured data. The influence of specimen unsupported length on Euler buckling is shown in figure 13. The buckling stress is very sensitive to unsupported length less than about 1.25 in (3.18 cm). The unsupported length of 1 inch (2.54 cm) appears to be reasonable in view of some tab debonding which was observed in the failed specimens (fig. 7). (3) Fiber compression failure (Equation (5)) predicts the highest value for longitudinal compression, about 46 percent higher than the average measured data.

Comparing the measured data and predictions in figure 12, it can be concluded that the specimens failed by flexure which is consistent with the stress-strain curve in figure 3. Using the average fracture strain of about 0.86 percent and the modulus of 15.6×10^6 psi (107 GPa) from table I, a longitudinal compression strength of 133 ksi (915 MPa) is predicted. This value is about 11 percent greater than that predicted by equation (2) (flexural/tensile). However, 133 psi (915 MPa) is only about 4 percent greater than the average measured strength of 128 ksi (890 MPa) in table I. The maximum, local compression stress at fracture, estimated from the corresponding maximum compression strain (1.2 percent) from figure 3, is 187 ksi (1290 MPa) which equals exactly that predicted by equation (5) for fiber compression failure.

The conclusion from the above discussion is that the AS/PR288 compression specimens failed by flexural failure mode triggered possibly by Euler buckling. Another conclusion is that the maximum local compressive stress at failure was induced by fiber compression failure.

The predicted longitudinal compression strengths using equations (1), (2), (3), and (5) for the T-300/5208 specimens and the measured data are summarized in figure 14. The measured data for these specimens divide into three groups. The specimens in the high strength group appear to have failed by fiber compression failure (eq. 5). The specimens in the middle strength group appear to have failed by either flexure (eq. (2)) or delamination (eq. (3)). The specimens in the lowest strength group appear to have failed by Euler buckling with an unsupported length of 2 inches (5.08 cm). An unsupported length of this dimension is excessive and would imply tab debonding of about 0.5 inch (1.27 cm) at each end. It could not be determined from the failed specimens whether tab debonding of this magnitude occurred though tab debonding was substantial.

The influence of unsupported length on Euler buckling for T-300/5208 is shown in figure 15. The buckling stress is very sensitive to unsupported length of less than 2.5 inches (6.35 cm). The curve in this figure shows that all the specimens could have failed by Euler buckling. For example, the unsupported length for the specimens in the high strength group was about 1.60 inch (4.06 cm) and that for the middle strength group was about 1.75 inch (4.44 cm). It is the closeness between these different failure modes which makes testing for longitudinal compression strength very difficult.

Using the average compression strain at fracture of 1.06 percent and a modulus of 19×10^6 psi (131 GPa) yields a longitudinal compression stress at fracture of 201 ksi (1380 MPa). This stress is very close to those predicted by the flexure and delamination failure modes (fig. 14). Using the average strain (about 1.6 percent) from figure 4 and the same modulus, a compression stress at fracture of 304 ksi (2100 MPa) is predicted. The corresponding maximum local compression stress at fracture is 332 ksi (2290 MPa). Both of these stress values are considerably higher than any measured values as well as the anticipated compressive strength based on the fiber compression failure mode. These high values indicate, to some extent, the nonlinearity of the stress-strain curve near fracture requiring use of tangent rather than initial modulus.

The major conclusion from the above discussion is that the T-300/5208 specimens failed in three different failure modes: (1) fiber compression for the high strength group (250 ksi (1720 MPa)); (2) flexure or delamination for the mid strength group (200 ksi (1380 MPa)); and (3) Euler buckling for the lowest strength group (150 ksi (1034 MPa)). Two other conclusions also follow from the above discussion. These are: (1) All specimens could have failed by Euler buckling and (2) longitudinal compression strengths of 250 ksi (1720 MPa) for T-300/5208 are obtainable experimentally.

Misalignment of the specimen in the compression fixture, fiber misalignment in the laminate and possible bending/stretching coupling also cause significant reductions in measured compression strength. Only specimen misalignment is reasonable. The other two imply fiber nonuniformity in the same laminate. If some fiber nonuniformity was present, the laminate as well as some specimens would have shown warpage and comparable reductions in the modulus (table I). No warpage was observed in either the laminates or the specimens cut therefrom. The moduli if anything are higher for the low strength group. Misalignment, on the other hand is not only possible but also quite probable since the stress/strain curves from the back-to-back gages show bending for the most part. The magnitude of the probable misalignment can be evaluated by estimating apparent eccentricities. The apparent eccentricities are estimated from the following equation:

$$\frac{e}{h} = \frac{1}{6}\left(\frac{S_{\ell 11C}}{S_a} - 1\right) \tag{6}$$

where e is the eccentricity, h is the specimen thickness, $S_{\ell 11C}$ is the "true" longitudinal compressive strength and S_a is the measured (apparent) compressive strength. Assuming a value of 250 ksi (1720 MPa) for $S_{\ell 11C}$, the e/h for the mid strength group (S_a = 200 ksi (1380 MPa)) is 0.042 (or an eccentricity of about 1-ply thickness assuming 5-mils ply thickness); that for the low strength group (S_a = 150 ksi (1034 MPa) is 0.111 (or an eccen-

tricity of about 2-ply thicknesses). Both of these eccentricities are quite reasonable indicating that the specimens failed by combined compression and bending. They also indicate the difficulties associated in eliminating these eccentricities in compressive testing. These kinds of eccentricities, on the other hand, would induce substantial bending in the specimen. The bending would have been picked up by the back-to-back strain gages. The back-to-back strain gage data from the low strength group specimens showed relatively less bending compared to the high strength group specimens (compare fig. 6 with fig. 4). Though these modes could induce longitudinal compression failure, it appears that Euler buckling with long unsupported length was the most likely failure mode for the low strength group specimens.

CONCLUSIONS

The significant conclusions from an investigation on the longitudinal compression behavior of unidirectional graphite/epoxy (AS/PR288, and T-300/5208) composites are as follows:

1. The failure mode for the AS/E composites appear to be delamination controlled by interlaminar shear.
2. The T-300/E composites exhibited three different strength groups. The high strength group specimens appeared to have failed by the fiber compression failure mode. The mid-strength group specimens appeared to have failed by either flexure or by delamination. The low strength group specimens appeared to have failed by Euler buckling with unsupported length running into the end tabs.
3. Longitudinal compression strength induced by the fiber compression failure mode appears to be an upper bound. Those predicted using either the flexure or the delamination failure modes appear to provide a lower bound.
4. An equation is described which can be used to obtain conservative estimates on the longitudinal compression strength knowing the longitudinal tensile and flexural strengths of the same composite system.
5. Scanning electron microscope observations of the fracture surface characteristics of specimens taken from the three different strength groups of T-300/5208 did not reveal significant differences to allow the association of specific fracture surface characteristics with unique fracture modes.
6. Experimental determination of longitudinal compressive strength is sensitive to possible tab debonding and load misalignment. However, even if these are present the test data can still be used in conjunction with theoretical analysis to determine a reasonable value for longitudinal compression strength.

REFERENCES

1. Chamis, C. C., "Micromechanics Strength Theories," Fracture and Fatigue, L. J. Broutman, Ed., Composite Materials Vol. 5, L. J. Broutman and R. H. Krock, Eds., Academic Press, New York, 1976, pp. 93-151.
2. Agarwal, B. D., and Broutman, L. J., Analysis and Performance of Fiber Composites, John Wiley and Sons, NY, 1980, pp. 15-69.
3. Cark, R. K. , and Lesagor, W. B., "Compression Testing of Graphite/Epoxy Composite Materials," Test Methods and Design Allowables for Fibrous Composites, ASTM STP-734, C. C. Chamis, Ed., American Society for Testing and Materials, 1981, pp. 34-53.

4. Shuart, M. J., "An Evaluation of the Sandwich Beam Compressions Test Method for Composites," Test Methods and Design Allowables for Fibrous Composites, ASTM STP-734, C. C. Chamis, Ed., American Society for Testing and Materials, 1981, pp. 152-165.
5. Grimes, G. C., "Experimental STudy of Compression - Compression Fatigue of Graphite/Epoxy Composites," Test Methods and Design Allowables for Fibrous Composites, ASTM STP-734, C. C. Chamis, Ed., American Society for Testing and Materials, 1981, pp. 281-340.
6. Chamis, C. C., Kring, J, and Sullivan, T. L., Automated Testing Data Reduction Computer Program. NASA TM X-68050, 1972.
7. Sinclair, J. H., and Chamis, C. C., Mechanical Behavior and Fracture Characteristics of Off-Axis Fiber Composites I - Experimental Investigation. NASA TP-1081, Dec. 1977.
8. Chamis, C. C., and Lark, R. F., "Non-Metallic Hybrid Composite Analysis, Design Application and Fabrication," Hybrid and Select Metal Matrix Composites: State-of-the-Art Review, W. J. Renton Ed., The American Institute of Aeronautics and Astronautics, NY, 1977, pp 13-16.
9. Chamis, C. C., Lark, R. F., and Sinclair, J. H., Mechanical Property Characterization of Intraply Hybrid Composites, NASA TM-79906, Prepared for the American Society for Testing and Materials Symposium, Dearborn, Michigan, October 2-3, 1979.

TABLE I. - SUMMARY OF MEASURED DATA, LONGITUDINAL COMPRESSION TESTS

Composite	Specimen number	Specimen thickness		Specimen width		Fracture stress		Fracture strain percent[a]	Compression modulus[a]		Poisson's ratio[a]
		in.	cm	in.	cm	ksi	GPa		10^6 psi	GPa	
AS/PR288 $[0]_{10}$	1	0.0555	0.141	0.2498	0.634	123	0.848	0.64	19.0	131	0.32
	2	.0553	.140	.2500	.635	135	.931	.90	12.7	88	[b].33
	3	.0551	.140	.2480	.630	122	.841	.82	16.2	112	.34
	4	.0550	.140	.2483	.631	145	1.000	.98	15.4	106	.35
	5	.0546	.139	.2481	.630	136	.938	.94	15.2	105	.35
	6	.0544	.138	.2487	.632	131	.903	.96	14.3	99	.34
	7	.0542	.138	.2483	.631	126	.869	.84	15.9	110	.30
	8	.0539	.137	.2489	.632	131	.903	.96	14.4	99	.36
	9	.0535	.136	.2483	.631	123	.910	.90	14.0	97	.34
	10	.0531	.135	.2488	.632	119	.820	.84	14.8	102	.34
	11	.0528	.134	.2490	.632	121	.834	.80	16.7	115	.38
	12	.0524	.133	.2487	.632	128	.882	.76	18.2	125	.36
	$\bar{X}$	0.0542	0.138	0.2487	0.632	128	0.890	0.86	15.6	107	0.34
	s	.0010	.003	.00063	.016	7.6	.052	.10	1.78	12.1	.02
T-300/5208 $[0]_{20}$	1	0.0970	0.246	0.260	0.660	172	1.19	1.00	18.0	124	0.32
	2	.0991	.252	.260	.660	253	1.74	1.54	17.8	123	.34
	3	.1004	.255	.260	.660	256	1.77	1.61	17.6	121	.34
	4	.1024	.260	.257	.653	244	1.68	1.52	17.6	121	.34
	5	.1036	.263	.256	.650	141	.97	[b].75	19.5	134	.30
	6	.1042	.265	.255	.648	151	1.04	.80	19.4	134	.31
	7	.1058	.269	.255	.648	220	1.52	1.24	18.8	130	.32
	8	.1059	.269	.255	.648	139	.96	.74	21.7	150	.35
	9	.1054	.268	.256	.650	206	1.42	1.15	18.8	130	.31
	10	.1064	.270	.255	.648	138	.95	.72	20.5	141	.32
	11	.1050	.267	.254	.645	166	1.14	.90	19.0	131	.33
	12	.1063	.270	.255	.648	145	1.00	.76	19.6	135	.33
	$\bar{X}$	0.1035	0.263	0.257	0.652	186	1.28	1.06	19.0	131	0.33
	s	.003	.008	.002	.005	47.0	.32	.34	1.23	8.5	.015

[a]Avg. of 2 gages (conv. factor: ksi x 0.68948×10^{-2} = GPa).
[b]1 gage.

TABLE II. - SELECTED PROPERTIES OF RESINS AND COMPOSITIES

Material	Density		Modulus		Tensile strength		Flexural strength		Short beam shear		Compression strength	
	lb/in^3	g/cc	10^6 psi	GPa	ksi	MPa	ksi	MPa	ksi	MPa	ksi	MPa
Resins:												
[a]PR288	0.0460	1.274	0.500	3.44	8.4	57.9	---	----	----	-----	----	----
[b]5208	.0458	1.267	.580	4.00	8.3	57.2	---	----	----	-----	----	----
Composites:												
[c]T-300/5208 (0.590 FVR)		-----	19	131	218	1503	310	2137	19.0	131	210	1448
[d]AS/PR288 (0.532 FVR)		-----	18.2	125	213.7	1473	230	1586	13.0	89.6	[d]170	1172

[a]3M data.
[b]Typical data.
[c]Reference 9.
[d]Reference 8.

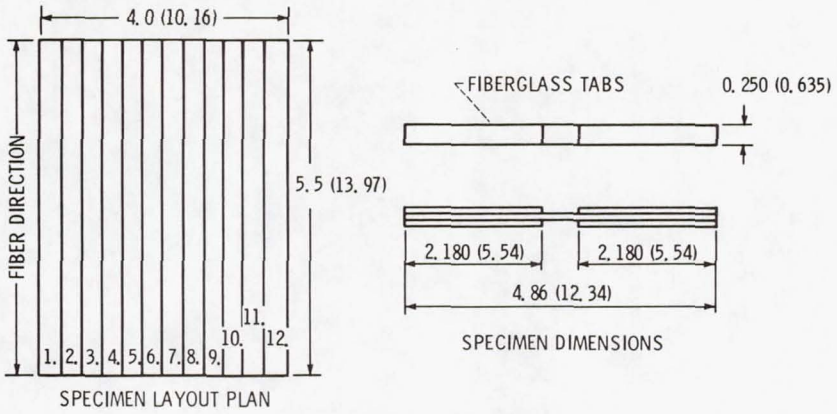

Figure 1. - Specimen layout plan and dimensions. (Dimensions in inches(cm).)

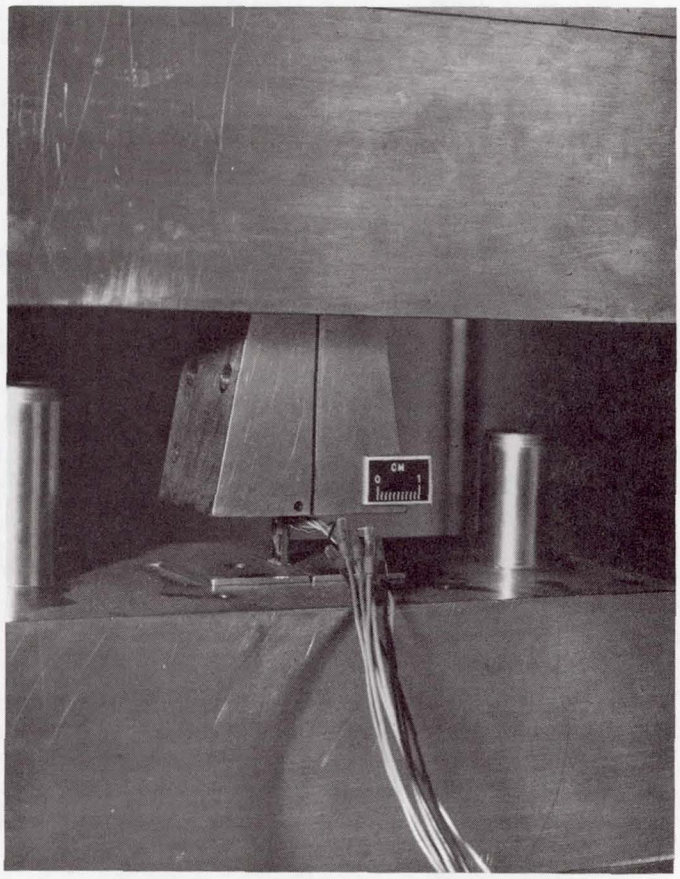

Figure 2. - Instrumented compression specimen in place.

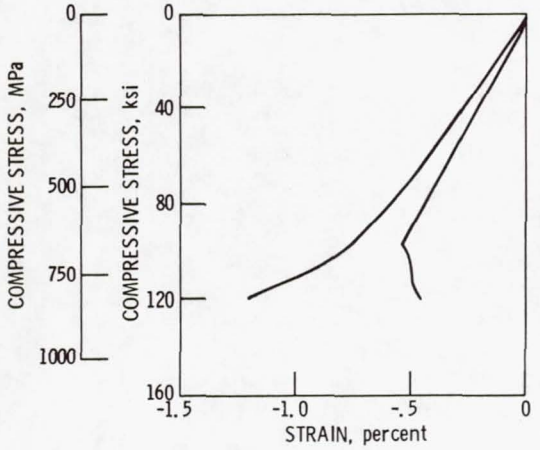

Figure 3. - Stress-strain curves for AS/PR288 specimen 10., table 1.

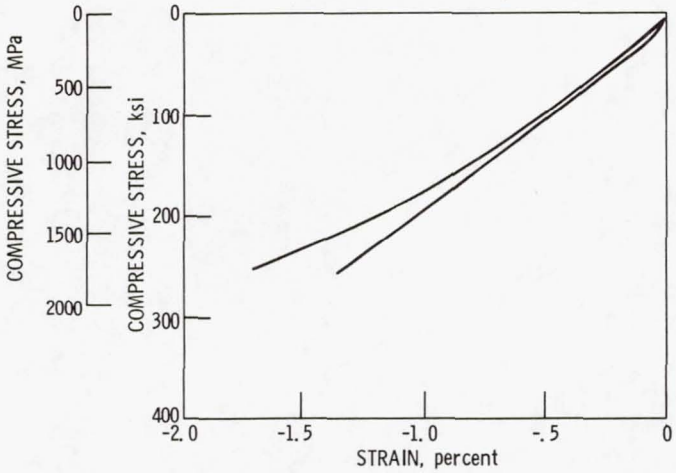

Figure 4. - Stress-strain curves for T-300/5208 specimen 2., table 1.

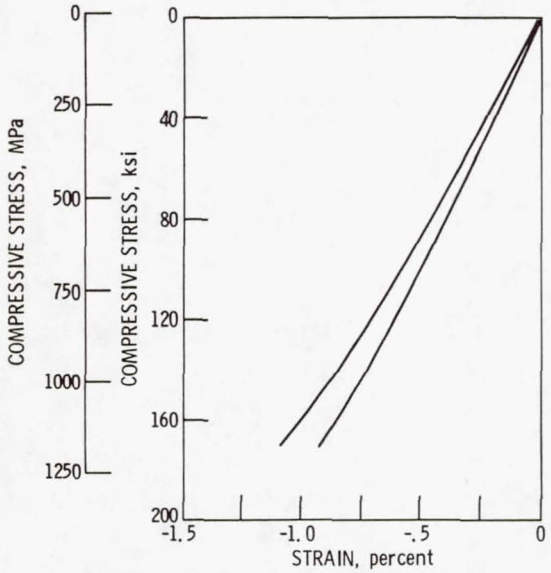

Figure 5. - Stress-strain curves for T-300/5208 specimen 1., table 1.

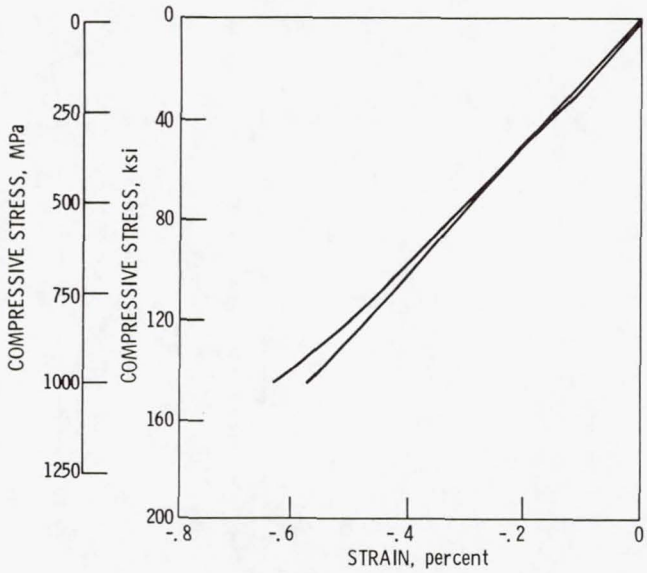

Figure 6. - Stress-strain curves for T-300/5208 specimen 12., table 1.

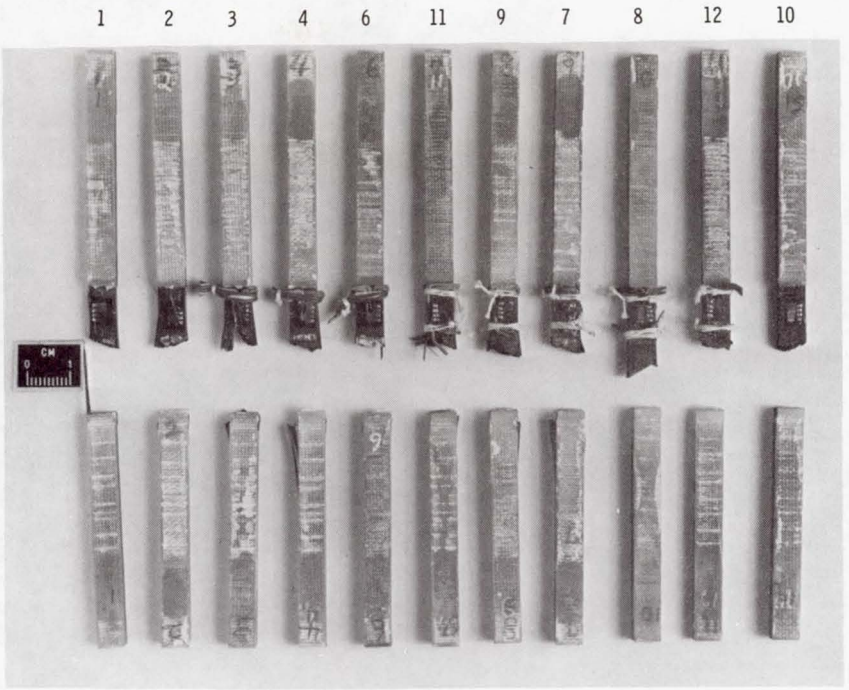

Figure 7. - Fractured T-300/5208 specimens.

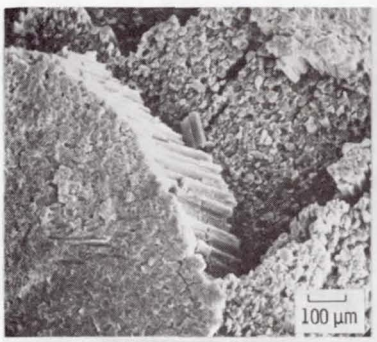

(a) General view.

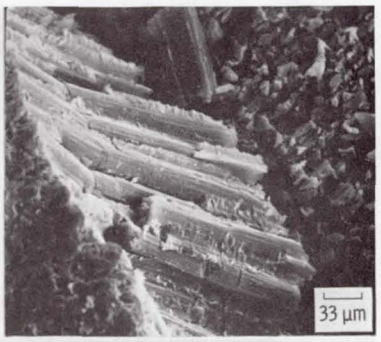

(b) Detailed view.

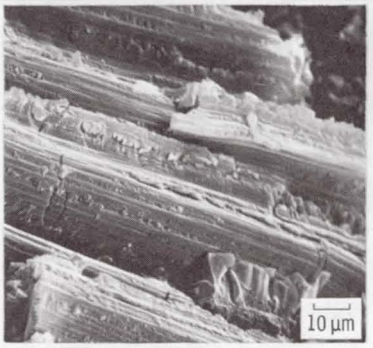

(c) Enlargement of detail to show fracture mode.

(d) Fracture.

Figure 8. - Scanning electron photomicrographs of fractured surface of T-300/5208 compression specimen (high-strength - 253 ksi (1740 MPa)).

C-80-5814

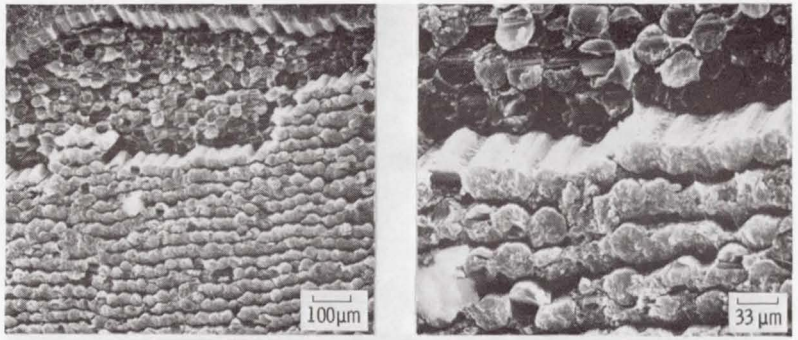

(a) General view. (b) Detailed view.

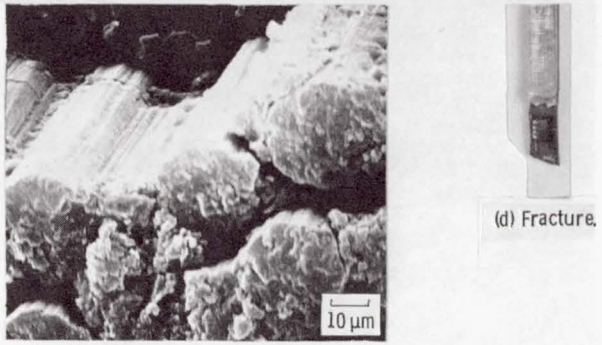

(c) Enlargement of detail to show fracture mode.

(d) Fracture.

Figure 9. - Scanning electron photomicrographs of fractured surface of T-300/5208 compression specimen (intermediate strength - 172 ksi (1190 MPa)).

C-80-5814

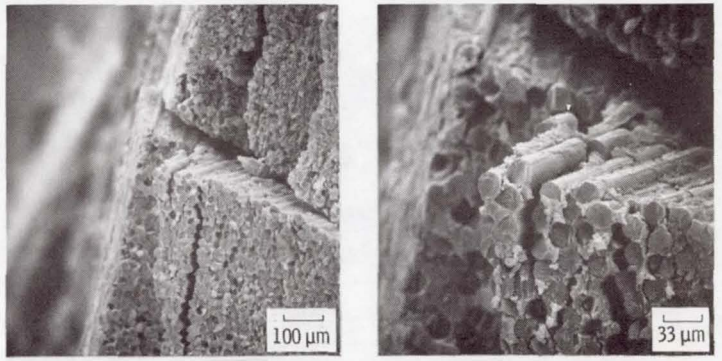

(a) General view. (b) Detailed view.

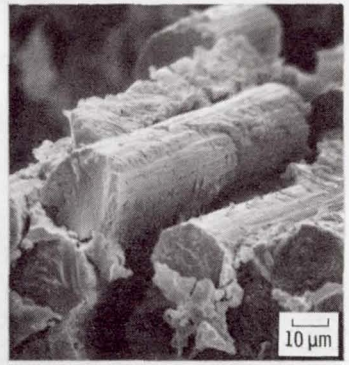

(c) Enlargement of detail to show fracture mode.

(d) Fracture.

Figure 10. - Scanning electron photomicrographs of fractured surface of T-300/5208 compression specimen (low-strength - 145 ksi (1000 MPa)).

C-80-5814

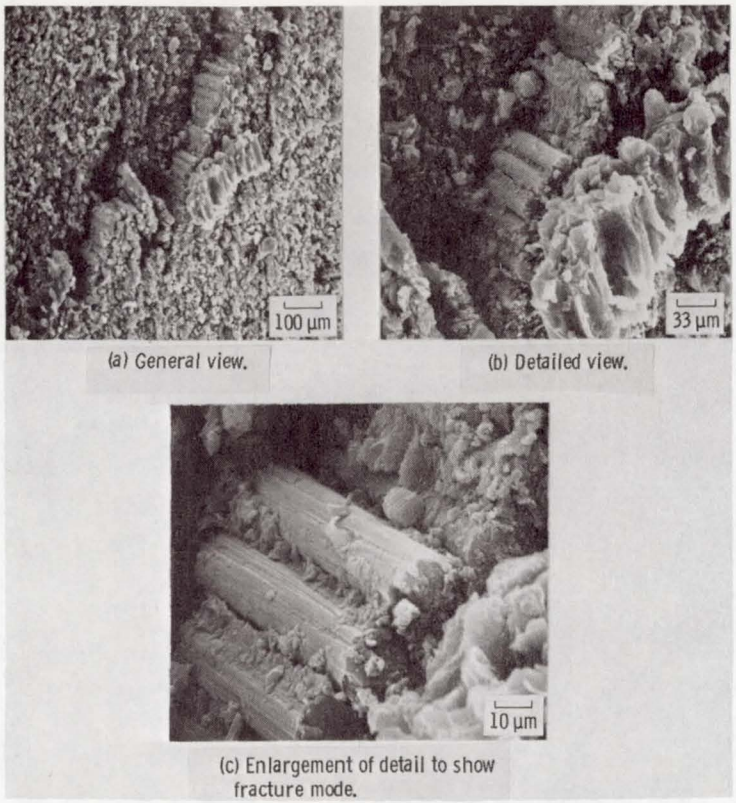

Figure 11. - Scanning electron photomicrographs of fractured surface of AS/PR288 compression specimen (strength - 119 ksi (820 MPa)).

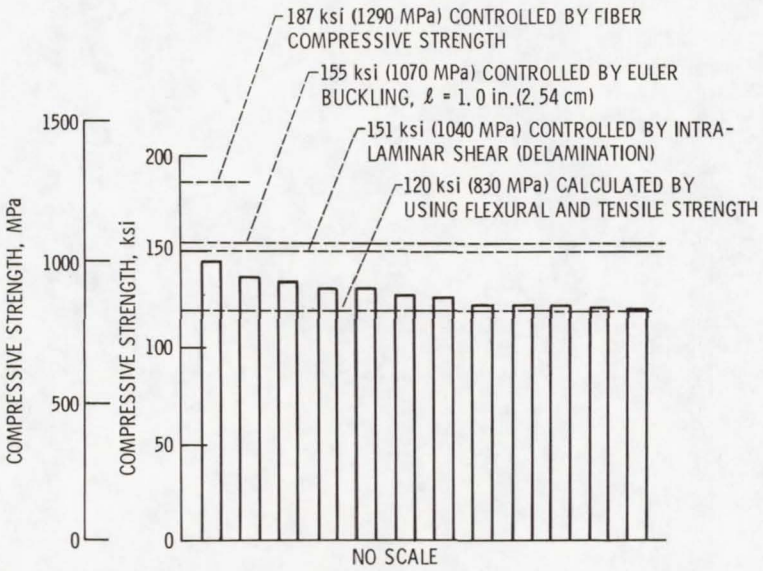

Figure 12. - Experimental compressive strength of AS/PR288 compared with predicted strengths.

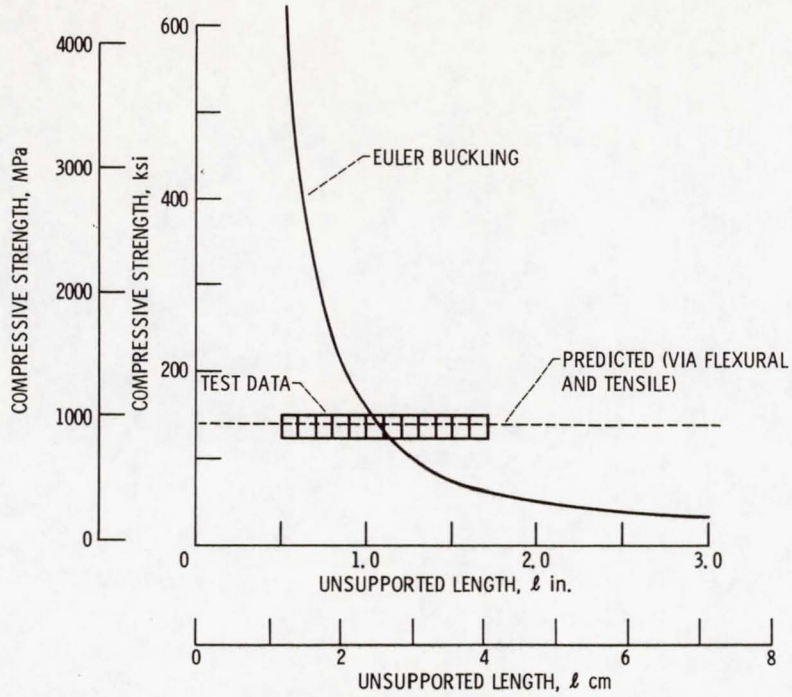

Figure 13. - Effect of unsupported gage length on compressive strength controlled by Euler buckling for AS/PR288.

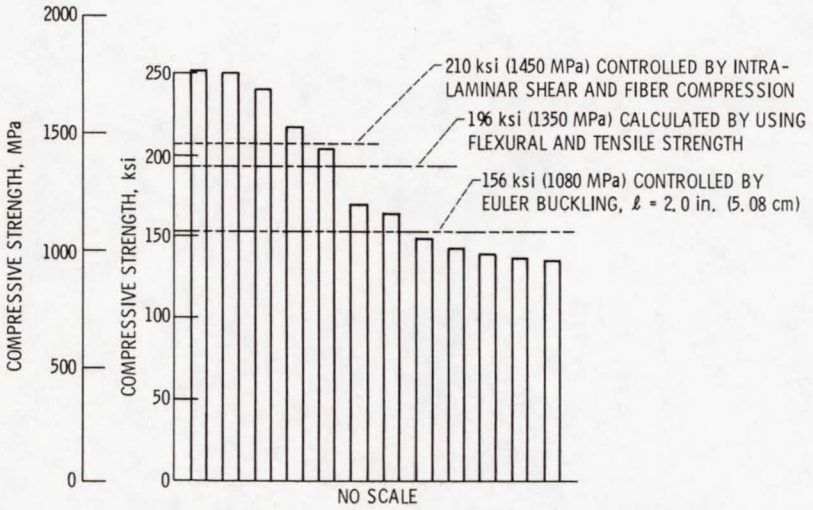

Figure 14. - Experimental compressive strength of T-300/5208 compared with predicted strengths.

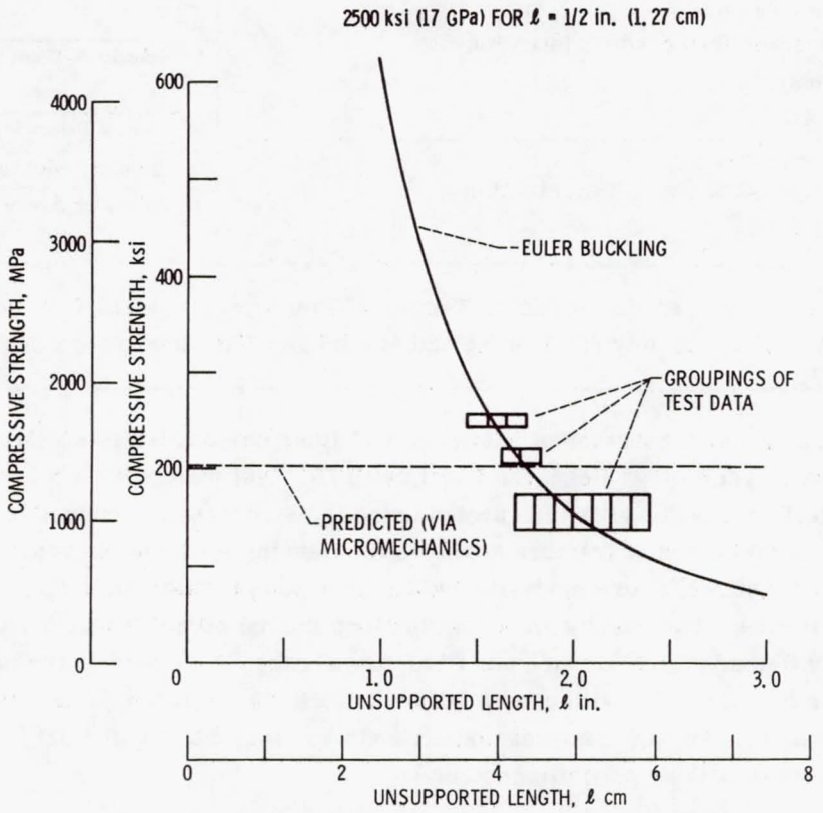

Figure 15. - Effect of unsupported gage length on compressive strength controlled by Euler buckling for T-300/5208.

1. Report No.	2. Government Accession No.	3. Recipient's Catalog No.
NASA TM-82833		

4. Title and Subtitle	5. Report Date
COMPRESSION BEHAVIOR OF UNIDIRECTIONAL FIBROUS COMPOSITES	6. Performing Organization Code 505-33-62
7. Author(s) J. H. Sinclair and C. C. Chamis	8. Performing Organization Report No. E-1145
9. Performing Organization Name and Address National Aeronautics and Space Administration Lewis Research Center Cleveland, Ohio 44135	10. Work Unit No.
	11. Contract or Grant No.
12. Sponsoring Agency Name and Address National Aeronautics and Space Administration Washington, D.C. 20546	13. Type of Report and Period Covered Technical Memorandum
	14. Sponsoring Agency Code

15. Supplementary Notes

Prepared for the Symposium on Compression Testing of Homogeneous Materials and Composites sponsored by the American Society for Testing and Materials, Williamsburg, Virginia, March 10-11, 1982.

16. Abstract

The longitudinal compression behavior of unidirectional fiber composites is investigated using the Illinois Institute of Technology Research Institute (IITRI) test method with thick and thin test specimens. The test data obtained is interpreted using the stress/strain curves from back-to-back strain gages, examination of fracture surfaces by scanning electron microscope and predictive equations for distinct failure modes including fiber compression failure, Euler buckling, delamination and flexure. The results show that the longitudinal compression fracture is induced by a combination of delamination, flexure and fiber tier breaks. No distinct fracture surface characteristics can be associated with unique failure modes. An equation is described which can be used to extract the longitudinal compression strength knowing the longitudinal tensile and flexural strengths of the same composite system.

17. Key Words (Suggested by Author(s))	18. Distribution Statement
Longitudinal compression; Test methods; Fiber composites; Unidirectional composites; Failure modes; Stress-strain curves; Scanning electron microscope; Predictive equations	Unclassified - unlimited STAR Category 24

19. Security Classif. (of this report)	20. Security Classif. (of this page)	21. No. of Pages	22. Price*
Unclassified	Unclassified		

* For sale by the National Technical Information Service, Springfield, Virginia 22161